

Reduced-Rank STAP Performance Analysis

C. D. PECKHAM, Member, IEEE

A. M. HAIMOVICH, Senior Member, IEEE

T. F. AYOUB

New Jersey Institute of Technology

J. S. GOLDSTEIN, Senior Member, IEEE

SAIC

I. S. REED, Fellow, IEEE

University of Southern California

The space-time radar problem is well suited to the application of techniques that take advantage of the low-rank property of the space-time covariance matrix. It is shown that reduced-rank (RR) methods outperform full-rank space-time adaptive processing (STAP) when the space-time covariance matrix is estimated from a data set with limited support. The utility of RR methods is demonstrated by theoretical analysis, simulations and analysis of real data. It is shown that RR processing has two opposite effects on the performance: increased statistical stability which tends to improve performance, and introduction of a bias which lowers the signal-to-noise ratio (SNR). A method for evaluating the theoretical conditioned SNR for fixed RR transforms is also presented. It is shown that while best performance is obtained using data-dependent transforms, the loss incurred by the application of fixed transforms (such as the discrete cosine transform) may be relatively small. The main advantage of fixed transforms is the availability of efficient computational procedures for their implementation. These findings suggest that RR methods could facilitate the development of practical, real-time STAP technology.

Manuscript received July 7, 1999; revised August 1, 1999; released for publication December 1, 1999.

IEEE Log No. T-AES/36/2/05237.

Refereeing of this contribution was handled by W. D. Blair.

Authors' current addresses: C. D. Peckham, Globix Corp., Network Engineering and Operations, New York City, NY; A. M. Haimovich, Center for Communications and Signal Processing Research, New Jersey Institute of Technology, Dept. of Electrical and Computer Engineering, University Heights, Newark, NJ 07102, E-mail: (haimovic@megahertz.njit.edu); T. F. Ayoub, AT&T; J. S. Goldstein, SAIC, 4001 North Fairfax Dr., Suite 400, Arlington, VA 22203-1616; I. S. Reed, Statistical Signal and Image Processing Lab, Dept. of Electrical Engineering, University of Southern California, Los Angeles, CA 90089-2565.

0018-9251/00/\$10.00 © 2000 IEEE

I. INTRODUCTION

Space-time adaptive processing (STAP) radar performance has been for some time a topic of considerable interest to the radar community. The need for adaptive methods arises in practice when statistical properties of the interference are not known and need to be inferred from the observed data. A primary difficulty in STAP is that the dimension of the adaptive weight vector can be large. As this dimension becomes larger, the required sample support to estimate noise-field statistics for STAP detection also needs to increase.

In optimum filter theory, the interference covariance is assumed known. This is not directly applicable to many practical problems, but it is the start from which adaptive filtering theory is developed. The optimal Neyman-Pearson detector for a known signal vector in colored Gaussian noise with a known covariance matrix is linear, i.e., it is constructed from a linear combination of the inputs to the space-time array. In practice, the interference-plus-noise covariance matrix is typically not known. A well-known approach under these conditions is the sample matrix inversion (SMI) method, which substitutes an estimate for the true noise covariance matrix expression in the linear detector [1]. It is also shown in [1] that if the sample support consists of a population of independent, identically distributed vectors with a multivariate Gaussian distribution, then the number of samples required to achieve performance within 3 dB of the optimal is approximately $K \approx 2N$, where N is the dimension of the vectors. The main drawback of the SMI detector is that its sample support K is proportional to the array degrees of freedom N . Recent publications have shown the advantages of various forms of reduced-rank (RR) processing over the full-rank SMI [2-4]. The sample support required by RR processing is independent of the array degrees of freedom and is given by $K \approx 2r$, where r is the rank of the interference to be rejected. Consequently, for $r \ll N$ and for the same sample support, the signal-to-interference plus noise (SINR)

A taxonomy of RR methods is shown in Fig. 1. Two main architectures are noted: the reduced-rank minimum variance beamformer (RR-MVB), and the reduced-rank generalized sidelobe canceler (RR-GSC). A third method, loaded SMI (LSMI), indicated by a dashed line, refers to adding a constant term to the diagonal of the covariance matrix to improve its numerical conditioning. LSMI behaves as a RR method [5, 6].

Given a rank-reducing transformation T , adaptation can take place in the subspace spanned by the principal components (PCs) of the transform (interference subspace methods) [4, 7, 8], or in the

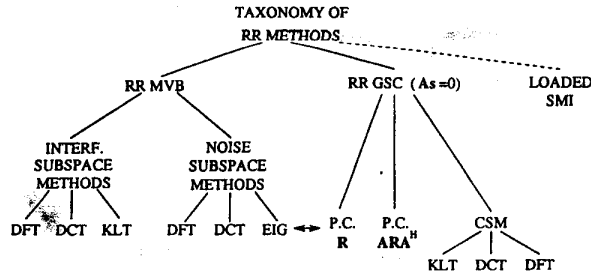


Fig. 1. Taxonomy of RR methods.

complementary subspace (noise subspace methods) [2, 3, 7, 8]. The transforms are either fixed (such as discrete Fourier transform (DFT), or discrete cosine transform (DCT)) or data dependent (Karhunen–Loeve transform (KLT)). Another class of RR-MVB and RR-GSC methods are based on the cross-spectral metric (CSM) [9, 10]. When the true covariance matrix is known, RR processing performance is less than or equal to full-rank performance. However, our interest in those methods stems from the fact that in limited data set regimens, RR methods actually *outperform* full-rank adaptive processing. This is explained by the presence, in addition to thermal noise effects, of errors resulting from the estimation process. RR processing suppresses estimation errors at the cost of a bias in the SNR. The net effect, however, is a significant performance improvement for cases when the interference may be modeled as low rank.

RR methods are clearly important for STAP radar, where a large number of degrees of freedom may be available. For a uniform array and for fixed pulse repetition frequency (PRF), the space-time clutter covariance matrix is essentially low rank due to the inherent oversampling nature of the STAP architecture. Hence, the space-time radar problem is well suited to the application of techniques that take advantage of the low-rank property. This work is organized as follows. Section II contains an analysis of RR processing when the covariance matrix is known. The case when the covariance matrix is estimated from the data is analyzed in Section III. Results are provided in Section IV for both simulated data and data from the DARPA mountain-top program. Finally, our conclusions are summarized in Section V.

II. REDUCED-RANK PROCESSING WITH KNOWN COVARIANCE

Consider a space-time array with ν antennas uniformly spaced and a κ coherent pulse interval (CPI) (Fig. 2). Data is collected from a 3D data cube which consists of the antenna elements, pulses of the CPI, and range returns as shown in Fig. 3. The determination as to whether a target is present at a range of interest is the goal of the signal processing.

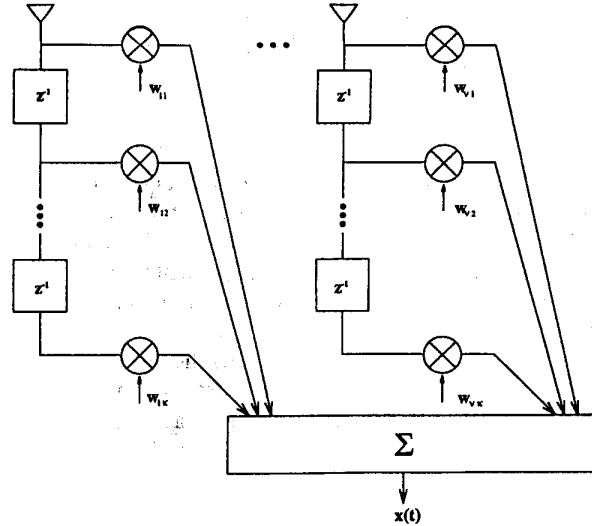


Fig. 2. STAP architecture.

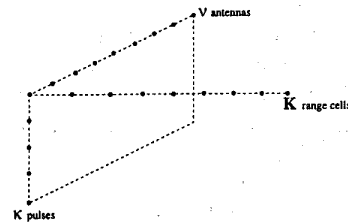


Fig. 3. STAP datacube.

To that end, an $N = \nu \times \kappa$ snapshot consisting of the 2D data slice at the range of interest, is processed to yield a decision statistic, which subsequently is compared to a threshold. Processing is carried out in the N -dimensional signal space resulting from stacking the snapshot column-wise. Radar detection is a binary hypothesis problem, where hypothesis \mathbf{H}_0 corresponds to target absence and \mathbf{H}_1 corresponds to target presence. Under hypothesis \mathbf{H}_0 , the $N \times 1$ received vector \mathbf{x} consists only of clutter \mathbf{c} and noise \mathbf{v} contributions:

$$\mathbf{x} = \mathbf{c} + \mathbf{v} \quad (1)$$

where \mathbf{x} is assumed a zero-mean, circularly symmetric Gaussian random vector with covariance matrix \mathbf{R} . Under hypothesis \mathbf{H}_1 , \mathbf{x} is given by

$$\mathbf{x} = a\mathbf{s} + \mathbf{c} + \mathbf{v} \quad (2)$$

where a is complex scalar representing the target signal amplitude and phase, and \mathbf{s} is the target vector. The target power is denoted σ_s^2 .

The colored noise covariance matrix $\mathbf{R} = E[(\mathbf{c} + \mathbf{v})(\mathbf{c} + \mathbf{v})^H]$, where the superscript denotes transpose and complex conjugate, is usually not known, hence an estimate is used instead. The estimate is derived from range cells in the vicinity of the tested range

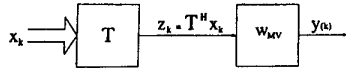


Fig. 4. RR-MVB.

cell (*secondary data*). The secondary data consists of clutter returns and, possibly, other interferences, such as jammers. The presence of narrowband jammers does not alter the signal model as presented, thus we restrict our attention only to clutter signals. The assumption is that the secondary data \mathbf{x}_k , $k = 1, \dots, K$, has the same statistical properties as the tested cell under hypothesis \mathbf{H}_0 . It is known that the covariance matrix of a well calibrated, uniform space-time array employing a fixed PRF is approximately low rank, i.e., it can be written

$$\mathbf{R} = \mathbf{Q}_1 \Lambda_1 \mathbf{Q}_1^H + \sigma^2 \mathbf{Q}_2 \mathbf{Q}_2^H \quad (3)$$

where the diagonal of the $r \times r$ matrix $\Lambda_1 = \text{diag}(\lambda_1, \dots, \lambda_r)$, $\lambda_1 \geq \lambda_2 \geq \dots \geq \lambda_r$, consists of the r principal (largest) eigenvalues of \mathbf{R} , the columns of \mathbf{Q}_1 are the corresponding eigenvectors, σ^2 is the variance of the white noise, and the columns of \mathbf{Q}_2 are the remaining eigenvectors of \mathbf{R} . The actual value of r is scenario dependent, but it is upper bounded by $r \leq \nu + \kappa - 1$, for equidistant sampling in space and time with a perfectly calibrated array [3].

This signal model suggests that STAP could benefit from the application of RR methods. Such methods may incur a loss in the SNR, but their main advantage lies in their statistical stability. RR methods with known covariance matrix are considered first, RR performance with unknown covariance is analyzed subsequently. The analysis is carried out in the frameworks of the MVB and the GSC processors.

A diagram of the reduced-rank MVB is shown in Fig. 4. The full-rank MVB weight vector is obtained as a solution to the optimization problem:

$$\min \mathbf{w}^H \mathbf{R} \mathbf{w} \quad \text{subject to} \quad \mathbf{s}^H \mathbf{w} = 1 \quad (4)$$

where $\mathbf{R} = E[\mathbf{x}_k \mathbf{x}_k^H]$, \mathbf{x}_k are snapshots of the secondary data, and \mathbf{s} is the steering vector. With RR-MVB, the vector \mathbf{x}_k is preprocessed by a full column rank $N \times r$ matrix transformation \mathbf{T} . The RR data is then the $r \times 1$ vector $\mathbf{z}_k = \mathbf{T}^H \mathbf{x}_k$, the RR covariance matrix is $\mathbf{T}^H \mathbf{R} \mathbf{T}$, and the RR steering vector is $\mathbf{t} = \mathbf{T}^H \mathbf{s}$.

The RR-MVB weight vector is the solution to

$$\min \mathbf{w}^H (\mathbf{T}^H \mathbf{R} \mathbf{T}) \mathbf{w} \quad \text{subject to} \quad (\mathbf{T}^H \mathbf{s})^H \mathbf{w} = 1 \quad (5)$$

and is given by the $r \times 1$ weight vector

$$\mathbf{w} = k (\mathbf{T}^H \mathbf{R} \mathbf{T})^{-1} \mathbf{T}^H \mathbf{s} \quad (6)$$

where k is a scalar chosen to satisfy the unit gain constraint in the direction of the desired signal.

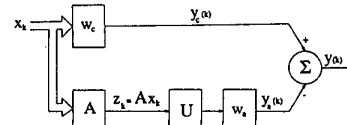


Fig. 5. RR-GSC.

Notice that the value of k does not affect the output SINR. The output SINR may be written as $\mu = |\mathbf{w}^H \mathbf{s}|^2 / \mathbf{w}^H \mathbf{R} \mathbf{w}$. Inserting the expression for the RR-MVB weight vector, the output SINR is given by

$$\mu = \mathbf{s}^H \mathbf{T} (\mathbf{T}^H \mathbf{R} \mathbf{T})^{-1} \mathbf{T}^H \mathbf{s} \quad (7)$$

where for notational convenience it is assumed that the target power is unity, $\sigma_s^2 = 1$.

The RR-GSC is shown in Fig. 5. The rank-reducing transformation is applied to the branch used for estimating the interference. From the figure it is observed that the output can be expressed

$$y = y_c(k) - y_a(k) = \mathbf{w}_c^H \mathbf{x}_k - \mathbf{w}_a^H \mathbf{U}^H \mathbf{A} \mathbf{x}_k \quad (8)$$

where \mathbf{w}_c , the weight vector of the nonadaptive portion, is just the steering vector $\mathbf{w}_c = \mathbf{s}$, \mathbf{w}_a is the adaptive weight, the matrix \mathbf{U} is a full column rank transformation, and \mathbf{A} is a transformation that blocks the look direction, $\mathbf{A} \mathbf{s} = \mathbf{0}$. Assuming that \mathbf{A} has full column rank, and that \mathbf{s} is the only vector in the null space of \mathbf{A} , the dimensions of \mathbf{A} are $(N-1) \times N$. Consequently, the rank-reducing matrix \mathbf{U} is $(N-1) \times r$. Multiple linear constraints can be incorporated in \mathbf{A} resulting in a null space of dimension equal to the number of constraints. The equivalent GSC weight vector can be written as

$$\mathbf{w} = \mathbf{w}_c - \mathbf{A}^H \mathbf{U} \mathbf{w}_a \quad (9)$$

The vector \mathbf{w}_a is found as the solution to the unconstrained optimization problem

$$\min_{\mathbf{w}_a} (\mathbf{s} - \mathbf{A}^H \mathbf{U} \mathbf{w}_a)^H \mathbf{R} (\mathbf{s} - \mathbf{A}^H \mathbf{U} \mathbf{w}_a) \quad (10)$$

This minimization results in

$$\mathbf{w}_a = (\mathbf{U}^H \mathbf{A} \mathbf{R} \mathbf{A}^H \mathbf{U})^{-1} \mathbf{U}^H \mathbf{A} \mathbf{R} \mathbf{s} \quad (11)$$

Using (9) and (11), the overall GSC weight vector is then given by

$$\mathbf{w} = (\mathbf{I}_N - \mathbf{A}^H \mathbf{U} (\mathbf{U}^H \mathbf{A} \mathbf{R} \mathbf{A}^H \mathbf{U})^{-1} \mathbf{U}^H \mathbf{A} \mathbf{R}) \mathbf{s} \quad (12)$$

where \mathbf{I}_N is the N -dimensional identity matrix. In [11] it is shown that for the MVB and GSC methods to be equivalent, the following conditions need to be met: 1) The matrix \mathbf{A} must block the look direction, $\mathbf{A} \mathbf{s} = \mathbf{0}$, and 2) $\mathbf{s}^H \mathbf{s} = 1$. In the case of the GSC, it can be shown that the output signal-to-noise ratio (SNR)

(when target power $\sigma_s^2 = 1$) is given by

$$\mu = (\mathbf{s}^H \mathbf{R} \mathbf{s} - \mathbf{s}^H \mathbf{R} \mathbf{A}^H \mathbf{U} (\mathbf{U}^H \mathbf{A} \mathbf{R} \mathbf{A}^H \mathbf{U})^{-1} \mathbf{U}^H \mathbf{A} \mathbf{R} \mathbf{s})^{-1}. \quad (13)$$

Various choices of the rank reducing transformation \mathbf{U} are now considered.

1) The goal is to maximize μ . In turn, this is achieved by maximizing the term

$$\eta = \mathbf{s}^H \mathbf{R} \mathbf{A}^H \mathbf{U} (\mathbf{U}^H \mathbf{A} \mathbf{R} \mathbf{A}^H \mathbf{U})^{-1} \mathbf{U}^H \mathbf{A} \mathbf{R} \mathbf{s}.$$

For a given reduced rank r , one way η may be optimized is by a transformation \mathbf{U} such that

$$\mathbf{A}^H \mathbf{U} = \mathbf{Q}_1 \quad (14)$$

where \mathbf{Q}_1 consists of the r principal eigenvectors of \mathbf{R} . Assuming that the $(N-1) \times N$ signal blocking matrix \mathbf{A} has full column rank, the elements of \mathbf{U} can be obtained from the solution of a least-squares problem. It is easy to show that with this choice of \mathbf{U} :

$$\begin{aligned} \mu &= (\mathbf{s}^H \mathbf{R} \mathbf{s} - \mathbf{s}^H \mathbf{Q}_1 \mathbf{\Lambda}_1 \mathbf{Q}_1^H \mathbf{s})^{-1} \\ &= (\mathbf{s}^H \mathbf{Q}_2 \mathbf{\Lambda}_2 \mathbf{Q}_2^H \mathbf{s})^{-1}. \end{aligned} \quad (15)$$

2) To avoid the complication of a least-squares problem, let the matrix \mathbf{U} be restricted to consist of r of the $(N-1)$ eigenvectors of $\mathbf{R}_a = \mathbf{A} \mathbf{R} \mathbf{A}$, where $\mathbf{R}_a = \mathbf{Q}_1 \mathbf{\Lambda}_1 \mathbf{Q}_1^H + \mathbf{Q}_2 \mathbf{\Lambda}_2 \mathbf{Q}_2^H$, and $\text{rank}(\mathbf{Q}_1) = r$. A natural choice would be to let the rank-reducing transformation consist of the r principal eigenvectors of \mathbf{R}_a , i.e., $\mathbf{U} = \mathbf{Q}_1$.

3) For a known covariance matrix \mathbf{R} , an optimal approach that maximizes the output SINR for a given rank r , is suggested in [9, 10]: construct \mathbf{U} from the r eigenvectors of \mathbf{R}_a that maximize the quantity

$$\frac{|\bar{\mathbf{q}}_i^H \mathbf{A} \mathbf{R} \mathbf{s}|^2}{\bar{\lambda}_i} \quad (16)$$

where $\bar{\mathbf{q}}_i$, $\bar{\lambda}_i$ are, respectively, eigenvectors and eigenvalues of \mathbf{R}_a . In the references, this method is referred as the CSM method.

4) PC decomposition, such as considered above, is data dependent. Fixed, RR transformations can be constructed by selecting the PCs of the DFT or the DCT. The CSM can also be used in conjunction with these fixed transforms [9, 10].

Next, rank-reducing transformations are evaluated in the MVB framework. Consider the SINR at the MVB output, as given by (7). When the transformation \mathbf{T} is unitary, it has no effect on the output SINR, and $\mu = \mathbf{s}^H \mathbf{R}^{-1} \mathbf{s} = \mu_{\max}$. For any $N \times r$ rank-reducing transformation \mathbf{T} , $r < N$, $\mu = \mathbf{s}^H \mathbf{T} (\mathbf{T}^H \mathbf{R} \mathbf{T})^{-1} \mathbf{T}^H \mathbf{s} \leq \mu_{\max}$. Specific examples are considered below.

1) Consider how case 1 of the GSC translates to the MVB framework. By substituting (14) in (12), we obtain the equivalent MVB weight vector

$$\mathbf{w} = (\mathbf{I}_N - \mathbf{Q}_1 \mathbf{Q}_1^H) \mathbf{s}. \quad (17)$$

This relation establishes an equivalence between the RR-GSC and the eigencanceler [3]. The eigencanceler is a method that produces the minimum norm weight vector meeting the set of linear constraints, and subject to the additional constraint of orthogonality to the interference subspace (formed by the principal eigenvectors of the space-time covariance matrix). Since $\mathbf{Q}_2 \mathbf{Q}_2^H = \mathbf{I}_N - \mathbf{Q}_1 \mathbf{Q}_1^H$, the eigencanceler is equivalent to the application of a rank-reducing transformation $\mathbf{T} = \mathbf{Q}_2$, where the columns of \mathbf{Q}_2 span the noise subspace of the covariance \mathbf{R} . Indeed, (17) is obtained by using $\mathbf{T} = \mathbf{Q}_2$ and substituting (3) in (6). The eigencanceler is useful when there is a sizable projection $\mathbf{Q}_2^H \mathbf{s}$. The output SINR is given by

$$\begin{aligned} \mu &= \mathbf{s}^H \mathbf{Q}_2 (\mathbf{Q}_2^H \mathbf{R} \mathbf{Q}_2)^{-1} \mathbf{Q}_2^H \mathbf{s} \\ &= \mathbf{s}^H \mathbf{Q}_2 \mathbf{\Lambda}_2^{-1} \mathbf{Q}_2^H \mathbf{s} \\ &\leq \mu_{\max} \end{aligned} \quad (18)$$

where

$$\mu_{\max} = \mathbf{s}^H \mathbf{Q}_1 \mathbf{\Lambda}_1^{-1} \mathbf{Q}_1^H \mathbf{s} + \mathbf{s}^H \mathbf{Q}_2 \mathbf{\Lambda}_2^{-1} \mathbf{Q}_2^H \mathbf{s}. \quad (19)$$

2) The $N \times r$ matrix is given by $\mathbf{T} = \mathbf{Q}_1$, i.e., it consists of the r PCs of the signal-plus-interference subspace [4]. In this case \mathbf{T} consists of the PCs of the KLT. The output SINR is given by $\mu = \mathbf{s}^H \mathbf{Q}_1 \mathbf{\Lambda}_1^{-1} \mathbf{Q}_1^H \mathbf{s}$. Note that if the look direction is in the noise subspace of the transform \mathbf{T} , i.e., $\mathbf{T}^H \mathbf{s} = \mathbf{0}$, there is no solution that meets the linear constraint in (6). This problem is circumvented in [12] by the augmentation of \mathbf{T} with the vector \mathbf{s} , $[\mathbf{T}, \mathbf{s}] \rightarrow \mathbf{T}$.

3) The columns of \mathbf{T} may be designed using the CSM approach, where the eigenvectors are enumerated in accordance with the magnitude of $|q_i^H \mathbf{s}|^2 / \lambda_i$.

4) Similar to case 4 of the GSC, the rank reducing transformation \mathbf{T} may be constructed from the PCs of a fixed transform such as the DFT or the DCT.

To reiterate, when the true covariance matrix \mathbf{R} is known, RR processing never exceeds the performance achievable by the full-rank processor. The strength of RR methods is revealed for unknown covariance. This case is considered in the next section.

III. REDUCED-RANK PROCESSING WITH UNKNOWN COVARIANCE

In practice, the space-time covariance matrix is not known and it needs to be estimated from the secondary data. This is an application for which RR methods can take advantage of their improved statistical stability. Let the number of snapshots from the secondary data set (sample support) be equal to K . Then the estimated covariance matrix is given by $\hat{\mathbf{R}} = (1/K) \sum_{k=1}^K \mathbf{x}_k \mathbf{x}_k^H$. In this section, the performance of RR processors is analyzed as a function of the sample support K .

A widely accepted measure of performance for radar systems is the probability of detection. In adaptive radar, detection probability is a function of the weight vector. Likewise, the weight vector is derived from estimates of the covariance matrix of the secondary data, and as such, its elements are random variables. This makes the detection probability dependent on the outcome of the sample covariance matrix. Insight can be gained by expressing detection probability as a function of the *conditioned SNR* (CSNR). The CSNR is defined as the effective SINR obtained by the application of a particular method, normalized by the optimal SINR (known covariance matrix, full-rank case):

$$\rho = \frac{\text{SINR}_{\text{eff}}}{\text{SINR}_{\text{opt}}} \quad (20)$$

The CSNR is a random variable, always bounded $0 \leq \rho \leq 1$. For a target signal amplitude of a and an array weight vector of \mathbf{w} , the effective SINR at the output is given by $\text{SINR}_{\text{eff}} = |a|^2 |\mathbf{w}^H \mathbf{s}|^2 / \mathbf{w}^H \mathbf{R} \mathbf{w}$. The optimal SINR is given by $\text{SINR}_{\text{opt}} = |a|^2 \mathbf{s}^H \mathbf{R}^{-1} \mathbf{s}$. It follows that for a particular method, the CSNR can be computed from

$$\rho = \frac{|\mathbf{w}^H \mathbf{s}|^2}{\mathbf{w}^H \mathbf{R} \mathbf{w}} \frac{1}{\mathbf{s}^H \mathbf{R}^{-1} \mathbf{s}} \quad (21)$$

Several specific methods are considered below. With SMI, the full-rank MVB weight vector is given by $\mathbf{w} = \hat{\mathbf{R}}^{-1} \mathbf{s}$. The density of the CSNR for the SMI method with Gaussian data has been derived in [1], and is given by the beta distribution with parameters K and N ,

$$f_\rho(\rho) = \frac{\Gamma(K+1)}{\Gamma(N-1)\Gamma(K+2-N)} (1-\rho)^{N-2} \rho^{K+1-N} \quad (22)$$

where $\Gamma(K) = (K-1)!$ is the standard gamma function. When a rank r , $r \leq N$, transformation \mathbf{T} is applied to the data, the CSNR can be written

$$\rho = \frac{(\mathbf{t}^H \hat{\Sigma}^{-1} \mathbf{t})^2}{\mathbf{t}^H \hat{\Sigma}^{-1} \Sigma \hat{\Sigma}^{-1} \mathbf{t} \mathbf{s}^H \mathbf{R}^{-1} \mathbf{s}} \quad (23)$$

where $\mathbf{t} = \mathbf{T}^H \mathbf{s}$ is an $r \times 1$ vector, and $\Sigma = \mathbf{T}^H \mathbf{R} \mathbf{T}$, $\hat{\Sigma} = \mathbf{T}^H \hat{\mathbf{R}} \mathbf{T}$ are $r \times r$ matrices. To allow for adaptation away from the interference subspace, the rank of the transformation \mathbf{T} needs to be $r \geq p+1$, where p is the rank of the interference subspace.

The distribution of ρ for various RR methods is now determined. Two classes of transformations are distinguished: 1) the class of fixed transformations, and 2) the class of data-dependent transformations. The former applies when \mathbf{T} is formed from data-independent transformations such as the DFT or the DCT. To the latter class belong data-dependent transformations \mathbf{T} such as formed by the eigenvectors of the estimated covariance $\hat{\mathbf{R}}$. The CSNR for each of these classes is subsequently analyzed.

Analysis of Fixed Transforms: For fixed \mathbf{T} , (23) can be rewritten

$$\rho = \rho_b \rho_r \quad (24)$$

where ρ_r is the RR CSNR,

$$\rho_r = \frac{(\mathbf{t}^H \hat{\Sigma}^{-1} \mathbf{t})^2}{\mathbf{t}^H \hat{\Sigma}^{-1} \Sigma \hat{\Sigma}^{-1} \mathbf{t} \mathbf{t}^H \Sigma^{-1} \mathbf{t}} \quad (25)$$

and ρ_b is the bias in the optimal SINR introduced by the transformation \mathbf{T} ,

$$\rho_b = \frac{\mathbf{t}^H \Sigma^{-1} \mathbf{t}}{\mathbf{s}^H \mathbf{R}^{-1} \mathbf{s}} \quad (26)$$

Relations (24)–(26) clearly demonstrate the effect of RR transformation on the SMI-MVB method. The linear transformation \mathbf{T} preserves the Gaussian distribution of the data, hence the RR CSNR ρ_r has a beta distribution with parameters K and r (i.e., the density in (22) with N replaced by r). Improved statistical stability is evident in the higher CSNR values associated with ρ_r . For example, for the full-rank SMI, $E[\rho] = 0.5$ for a number of snapshots $K = 2N - 3$ [1], while for the RR SMI, $E[\rho_r] = 0.5$ for $K = 2r - 3$, i.e., fewer samples are required for the same performance level. The higher CSNR values due to improved statistical stability, are somewhat offset by the bias term ρ_b , which is the loss in the optimal SINR due to the rank reduction for known covariance matrix. This loss is the quantity μ/μ_{max} analyzed in the previous section. The density of ρ is then given in terms of the density of ρ_r by the expression:

$$f_\rho(\rho) = \frac{1}{\rho_b} f_{\rho_r} \left(\frac{\rho}{\rho_b} \right), \quad 0 \leq \rho \leq \rho_b. \quad (27)$$

It is interesting to note that the linearly constrained (Frost-type) SNR maximization problem also has a rank reduction property and the corresponding CSNR has the same distribution as (22) with N replaced by $N - n + 1$, where n is the number of linear constraints on the weight vector [13].

The performance of the GSC processor with a fixed rank-reducing transformation is analyzed in [14].

Analysis of Data Dependent Transforms: The case when \mathbf{T} is data dependent cannot be directly derived from the SMI distribution. In this case \mathbf{T} is a random matrix and its effect on the CSNR needs to be evaluated statistically. The weight vector may be constrained to lie either in the noise subspace or the interference subspace.

The method resulting from the noise subspace constraint is referred to as the principal components inverse (PCI) in [2, 7, 8] and as eigencanceler in [3]. The weight vector is given by

$$\mathbf{w} = (\mathbf{I}_N - \hat{\mathbf{Q}}_1 \hat{\mathbf{Q}}_1^H) \mathbf{s}. \quad (28)$$

The CSNR density function for the eigencanceler was derived in [15]. The derivation is based on the

asymptotic expansion of the distribution of the PCs of the covariance matrix. Therein it is shown that, unlike the SMI density in (22), for the eigencanceler, the density depends on the covariance matrix. It is noted in [15] that the expression in (29) below was developed under the assumption that the projection of the steering vector \mathbf{s} on the true interference subspace is negligible compared with its projection on the true noise subspace, i.e., $\rho_b \simeq 1$. Retracing some of the steps in [15], it is not difficult to show that when this assumption is not imposed, the CSNR can be expressed in the form $\rho = \rho_b \rho_r$ (as in (24)), with $\rho_b = \mathbf{s}^H \mathbf{Q}_2 \mathbf{Q}_2^H \mathbf{s}$, and the density of ρ_r given by

$$f_{\rho_r}(\rho_r) = K \rho_r^{-2} \sum_{i=1}^p \frac{\pi_i}{\bar{\nu}_i} \exp\left(\frac{-K\left(\frac{1}{\rho_r} - 1\right)}{\bar{\nu}_i}\right), \quad 0 \leq \rho_r \leq \rho_b \quad (29)$$

where $\pi_i = \prod_{j=1, j \neq i}^r \bar{\nu}_j / (\bar{\nu}_j - \bar{\nu}_i)$, and $\bar{\nu}_i = \lambda_i^2 (\lambda_i - \sigma^2)^{-2}$, $i = 1, \dots, p$. For large interference-to-noise ratios, this expression simplifies to

$$f_{\rho_r}(\rho_r) = \frac{K^p}{\Gamma(p)} e^{-K(1-\rho_r)} (1 - \rho_r)^{p-1}. \quad (30)$$

The density of the CSNR $f_{\rho}(\rho)$ can then be computed as in (27). The density of PCI's CSNR is similar in form to that of the SMI method, with the difference that in (22) the signal dimensionality N is replaced by the quantity $(r = p + 1)$, [16]:

$$f_{\rho}(\rho) = \frac{\Gamma(K+1)}{\Gamma(p)\Gamma(K+1-p)} (1 - \rho)^{p-1} \rho^{K-p}. \quad (31)$$

The relation between (30) and (31) is explored in Appendix A. In the introduction it was mentioned that LSMI is essentially an RR technique. Indeed, a CSNR distribution similar to (31) is found in [6].

To complete the analysis of data-dependent transforms, we now consider the case of the weight vector constrained to the interference subspace. We refer to this method as principal components SMI (PC-SMI). Ignoring a constant gain, the PC-SMI weight vector is given by

$$\mathbf{w} = \hat{\mathbf{Q}}_1 \hat{\Lambda}_1^{-1} \hat{\mathbf{Q}}_1^H \mathbf{s} \quad (32)$$

where $\hat{\Lambda}_1$ is a diagonal matrix of the r principal eigenvalues of $\hat{\mathbf{R}}$, and the columns of $\hat{\mathbf{Q}}_1$ are the associated eigenvectors. Consistent with the earlier discussion on the topic, r is chosen larger than the actual interference subspace rank p . Direct analysis of PC-SMI's performance is very difficult since the CSNR is a function of both random eigenvalues and random eigenvectors. However, an approximation can be obtained based on the following argument. Let

$\hat{\mathbf{Q}}_1 = [\hat{\mathbf{Q}}_p \ \hat{\mathbf{q}}_r]$, and $\hat{\Lambda}_1 = \text{diag}(\hat{\Lambda}_p \ \hat{\lambda}_r)$, where $\hat{\mathbf{Q}}_p$ and $\hat{\Lambda}_p$ are, respectively, the eigenvectors and eigenvalues of the rank p interference, $r = p + 1$, and $\hat{\mathbf{q}}_r$, $\hat{\lambda}_r$ are the index r (in descending order) eigenvector and eigenvalue. Then the PC-SMI weight vector can be expressed

$$\mathbf{w} = \hat{\mathbf{Q}}_p \hat{\Lambda}_p^{-1} \hat{\mathbf{Q}}_p^H \mathbf{s} + \hat{\lambda}_r^{-1} \hat{\mathbf{q}}_r \hat{\mathbf{q}}_r^H \mathbf{s}. \quad (33)$$

For large interference eigenvalues, the elements of $\hat{\Lambda}_p^{-1}$ are negligible, and (33) can be approximated with

$$\mathbf{w} \simeq \hat{\lambda}_r^{-1} \hat{\mathbf{q}}_r \hat{\mathbf{q}}_r^H \mathbf{s}. \quad (34)$$

Since the vector $\hat{\mathbf{q}}_r$ is the noise subspace with respect to the rank p interference, this PC-SMI is equivalent to a noise subspace canceler. Thus under the assumption that the interference eigenvalues are very large, the density of ρ_r is given by (30). The overall CSNR is $\rho = \rho_b \rho_r$. For PC-SMI, $\rho_b = \mathbf{s}^H \mathbf{Q}_2 \mathbf{Q}_2^H \mathbf{s}$ is the projection of the steering vector \mathbf{s} onto the eigenvector \mathbf{q}_r . For the eigencanceler $\rho_b = \mathbf{s}^H \mathbf{Q}_2 \mathbf{Q}_2^H \mathbf{s}$, where $\mathbf{Q}_2 = [\mathbf{q}_r, \mathbf{q}_{r+1}, \dots, \mathbf{q}_{N_r}]$. Now, since $\mathbf{s}^H \mathbf{Q}_2 \mathbf{Q}_2^H \mathbf{s} \geq \mathbf{s}^H \mathbf{q}_r \mathbf{q}_r^H \mathbf{s}$, and the ρ_r s are the same, it would seem that the eigencanceler would always be preferable. This conclusion however is based on the assumption that the elements of $\hat{\Lambda}_p^{-1}$ are negligible. In general, PC-SMI is recommended when the steering vector lies mostly in the interference subspace, and conversely, when the steering vector is mainly in the noise subspace, the eigencanceler method should be applied.

IV. NUMERICAL RESULTS

Numerical results presented in this section were derived from computer simulations as well as from processing real data collected by the DARPA sponsored Mountain Top program.

The simulation model used an $\nu = 8$ element array with $\kappa = 4$ taps at each element. The clutter was located in the angular sector of 0 to 30 deg. The input clutter-to-noise ratio (CNR) was 10 dB at each antenna. In Figs. 6, 7, and 10, two jammers were located at 15 and 20 deg with a jammer-to-noise ratio (JNR) of 10 dB at each antenna. The interference subspace rank is bound by $r \leq \nu + \kappa - 1 = 11$. The bound would be achieved for interference that covers the full space-Doppler domain. For the sample covariance matrix used in the simulation, the clutter does not cover the whole space-Doppler domain and the interference rank was found to be 6. The steering vector was set at 50 deg, and at a normalized Doppler frequency of 0.4. The effect of the assumed rank p of the interference subspace on the average CSNR is shown in Fig. 6. For each method, the CSNR was computed from (21). The eigencanceler's weight vector used in (21) is given by (28). For the DCT and DFT RR transformations, \mathbf{T} was constructed from the steering vector \mathbf{s} , and the vectors

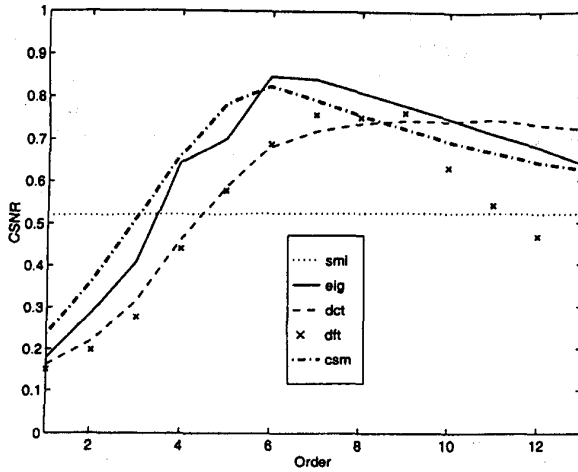


Fig. 6. CSNR versus rank order.

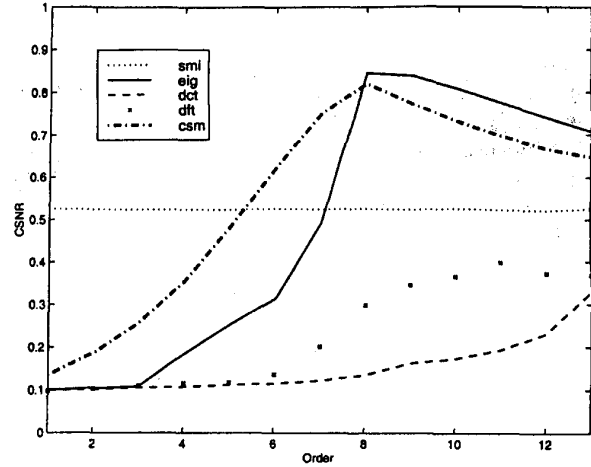


Fig. 8. CSNR versus rank order with large clutter field.

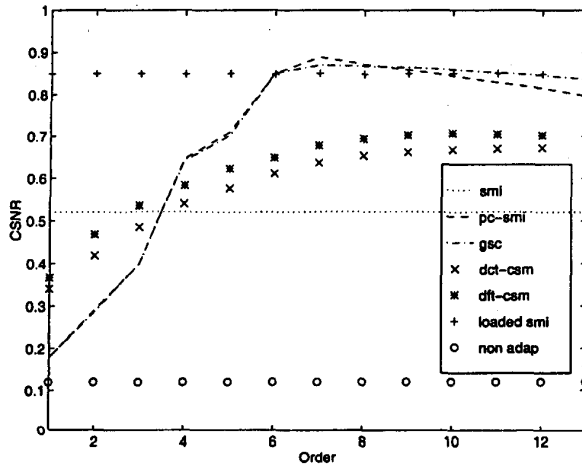


Fig. 7. CSNR versus rank order for other techniques.

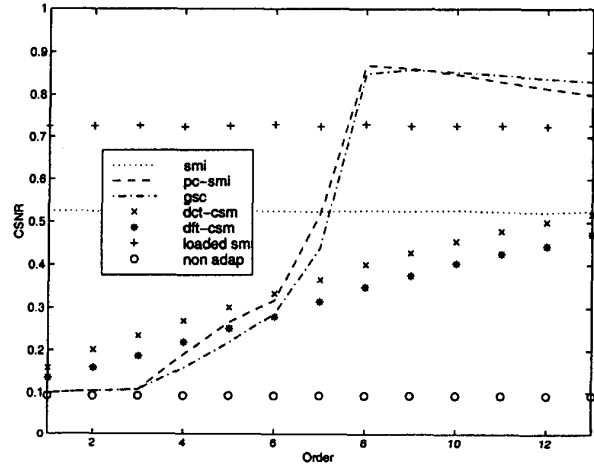


Fig. 9. CSNR versus rank order for other techniques with large clutter field.

corresponding to the p PCs of each transformation. The CSNR was computed from (23). In case of the CSM method, the matrix \mathbf{U} was constructed as in (16) substituting estimated values for unknown quantities. The CSM weight vector was subsequently evaluated from (12). The curves shown represent averages of 2000 runs. CSM provides slightly better performance when the rank is underestimated. The DCT-based method seems to be the least affected by overestimating the rank of the interference subspace. For the particular scenario considered, the eigencanceler and CSM methods peak near an interference subspace rank of $p = 6$, the true rank of the interference subspace. The DCT method peaks near an interference subspace rank of $p = 8$ while the DFT method peaks near an interference subspace rank of $p = 7$. The different rank values required by each method for best performance, are indicative of different capabilities to concentrate the power in a few principal values.

Several other methods are compared in Fig. 7: PC-SMI, RR-GSC, DFT-based CSM, and DCT-based CSM [9, 10]. The PC-SMI weight vector was computed from (32). The RR-GSC weight vector was evaluated using (12), where the matrix \mathbf{U} consisted of the p principal eigenvectors of $\hat{\mathbf{R}}_a = \mathbf{A}\hat{\mathbf{R}}\mathbf{A}^H$. The CSM methods shown in the figure are not discussed here; details on those methods can be found in [9, 10]. At their respective optimal rank orders, the CSNR peak values for the eigencanceler, CSM, PC-SMI and RR-GSC are in close agreement.

In Figs. 8 and 9 the clutter was located in the angular sector of 0 to 180 deg. The CNR per channel was 10 dB. The construction of \mathbf{T} and \mathbf{U} for the various techniques was performed as for Figs. 6 and 7. As shown in the figures, the peak for the eigencanceler, CSM, RR-GSC, and PC-SMI occur at a rank of $p = 8$. As expected, the more extended clutter leads to a larger number of principal values. As in the other simulations, the eigencanceler, CSM, PC-SMI,

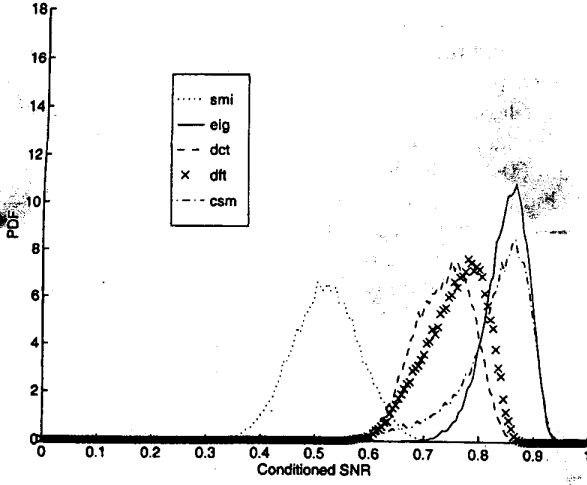


Fig. 10. Probability density of CSNR.

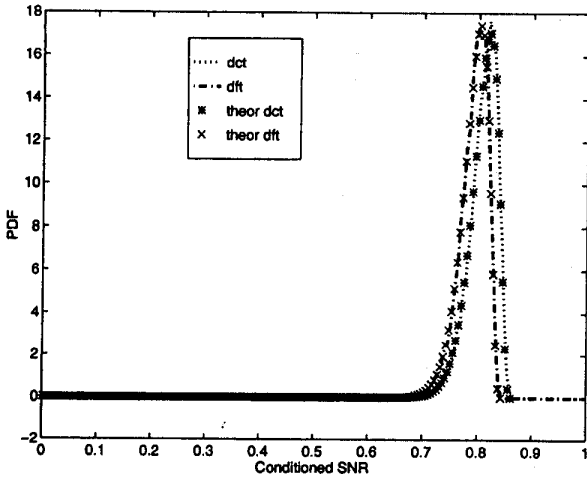


Fig. 11. Theoretical and simulated CSNR for DCT and DFT.

and RR-GSC are in close agreement. The DCT and DFT RR transformations do not perform as well in this scenario. This is due to the lower capability of these techniques to concentrate the clutter power in a limited number of principal values.

In Fig. 10, the distribution of ρ based on 20,000 runs is shown for several RR methods, as well as for full-rank SMI. The RR methods are: eigencanceller, DCT, DFT, and CSM based on the eigendecomposition and implemented as a GSC. The number of PCs used to generate the results shown in the figure is $p = 6$ for the eigencanceller and CSM, $p = 7$ for the DFT, and $p = 8$ for the DCT. The highest CSNRs are exhibited by the CSM and eigencanceller methods, with RR-MVB based on the DCT and DFT providing slightly lower performance. All RR methods clearly outperform the full-rank SMI.

As shown in Section III, the DCT and the DFT RR CSNR, ρ_r , have a beta distribution. The simulated CSNR of the DCT and the DFT RR cases may be

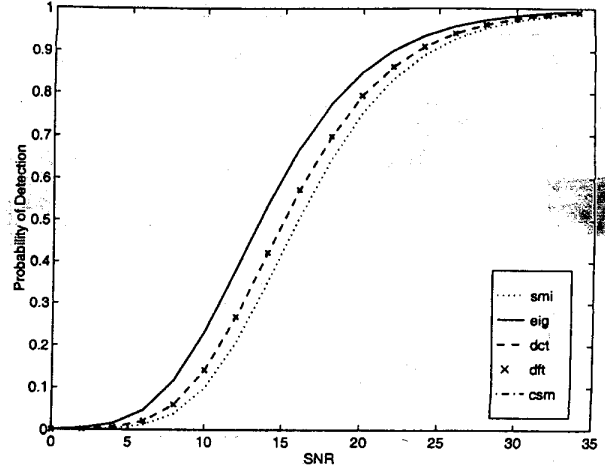


Fig. 12. Probability of detection for RR methods.

compared with the theoretical CSNR using (24). In Fig. 11, the simulated and theoretical CSNR results for both the DCT and DFT are shown. There is good agreement between the theoretical results and the simulations

Fig. 12 shows the average probability of detection. To compute the probability of detection, we make the assumption that the target amplitude a in (2) is a zero-mean, circularly symmetric complex Gaussian random variable with variance σ_s^2 . The test statistic is given by $y(k) = |\mathbf{w}^H \mathbf{x}(k)|^2$. Under \mathbf{H}_0 , $y(k)$ has an exponential distribution with density $f_y(y) = (1/\bar{y})e^{-y/\bar{y}}$, where $\bar{y} = E[y] = \mathbf{w}^H \mathbf{R} \mathbf{w}$. Setting the weight vector gain in (21) such that $|\mathbf{w}^H \mathbf{s}|^2 = 1$, we have $\bar{y} = 1/\rho\alpha$, where $\alpha = \mathbf{s}^H \mathbf{R}^{-1} \mathbf{s}$. The probability of false alarm conditioned on the CSNR ρ is given by

$$\begin{aligned} P_f(\rho) &= \int_{-\infty}^{y_T} f_y(y) dy \\ &= e^{-\rho\alpha y_T} \end{aligned} \quad (35)$$

where y_T is the detection threshold. The average probability of false alarm is given by

$$P_f = \int_0^1 P_f(\rho) f_\rho(\rho) d\rho \quad (36)$$

where $f_\rho(\rho)$ is the density of CSNR, which depends on the STAP method applied. Under \mathbf{H}_1 , $y(k)$ has an exponential distribution with parameter $\bar{y} = E[y] = \sigma_s^2 + \mathbf{w}^H \mathbf{R} \mathbf{w} = \sigma_s^2 + 1/\rho\alpha$. It follows that the conditional probability of detection is given by

$$P_d(\rho) = \exp \frac{-\rho\alpha y_T}{1 + \rho\alpha\sigma_s^2}. \quad (37)$$

The average probability of detection is then expressed

$$P_d = \int_0^1 P_d(\rho) f_\rho(\rho) d\rho. \quad (38)$$

In the simulations, we found the threshold $y_T(\rho)$ such that $P_f(\rho) = 10^{-5}$ and averaged the thresholds over

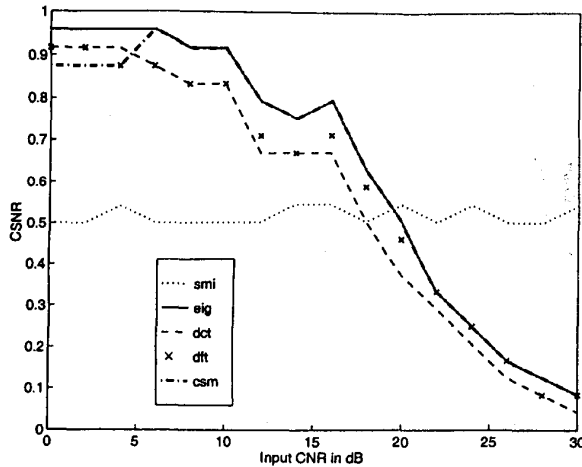


Fig. 13. CSNR versus CNR.

200 runs to obtain an average threshold value. This value was then used to compute $P_d(\rho)$ as a function of the SNR. For each SNR and each method, 200 values of $P_d(\rho)$ are averaged to serve as a point on the curves in Fig. 12. The figure illustrates the same trends as Fig. 10; best detection performance is provided by the eigencanceler and CSM, followed by DCT and DFT (indistinguishable), and finally the full-rank SMI. The effect of the CNR on performance is illustrated in Fig. 13. The CSNR is plotted as a function of the input CNR. The CSNR is computed for a rank-reducing transformation with $r = 4$. As the CNR increases, the interference power spills over more than 3–4 principal values. Thus the rank-reducing transformations are inadequate in capturing the interference power and performance is degraded.

Mountain-Top Data: The performance of the various RR methods are compared with one another when applied to the Mountain-Top data set. This data was collected from commanding sites (mountain tops) and radar motion is emulated using a technique developed at Lincoln Laboratories [17]. The sensor consists of 14 elements and the data is organized in CPIs of 16 pulses. For the data set analyzed here, the clutter was located around 245 deg azimuth and the target was at 275 deg and at a Doppler frequency of 156 Hz. A synthetic target was introduced in the data at 275 deg and 156 Hz. Note that the clutter and target have the same Doppler frequency, hence separation is possible only in the spatial domain. The target is not detectable without processing. The data analyzed was post-Doppler processing. A 16×14 matrix was formed for each range cell, where the temporal information is in the matrix columns, and the spatial information is contained in the rows. The received signals were processed using fixed Doppler filters. The filter containing the target and clutter was selected for follow-up processing and spatial processing was applied to 14×1 data vectors.

Fig. 14 shows the output of the various RR methods at the range cells for which data is available. The output power is measured relative to the skynoise power level, which was computed from separate files in the data set. The covariance matrix was estimated from 60 samples in the 150–159 km range, not including the 5 samples around the target range of 154 km. Each of the RR methods was evaluated utilizing four principal values (plus the steering vector in the case of the DCT and the DFT). For comparison purposes, the curve representing the unadapted data is also shown in Fig. 14(b). The unadapted weight vector was taken equal to the steering vector ($\mathbf{w} = \mathbf{s}$). The target is clearly not detectable without adaptive processing.

Fig. 15 displays the echo magnitude at the target range cell and for the beamforming at various angles. The figure was generated by scanning the steering angle over the angular sector indicated by the abscissa. The gain of each technique is measured with respect to the output when the beamformer points in the actual target direction (at 275 deg). This plot emulates the search mode of the radar. In the case presented, the eigencanceler and the CSM patterns are very similar to one another. Near the target angle, the DFT and the SMI are also at a maximum. The DCT pattern is at a maximum close to the target angle, but not directly on the steering angle. This is due to the number of DCT terms used and the training data utilized in the formation of the covariance matrix in this simulation.

Typically, the cell under test as well as cells in its vicinity are not included in the estimate of the covariance matrix. This implies a cumbersome procedure as different covariance matrices need to be associated with different range cells. Robust methods such that the same covariance matrix can be used for all range cells are of practical interest. If the target signal is included in the covariance, target cancellation may occur to the extent that the presumed steering vector is different from the true target vector. Differences between the steering vector and the true target vector may occur due to either pointing or calibration errors. Indeed, assume that the steering vector \mathbf{s} is precisely the target vector. Let the covariance matrix without the target contribution be \mathbf{R} , and with the target be \mathbf{R}_1 . Then $\mathbf{R}_1 = \mathbf{P}\mathbf{s}\mathbf{s}^H + \mathbf{R}$. It is easy to show that the SMI weight vector will remain unchanged (up to a gain factor). Hence, inclusion of the target in this case has no impact on the array performance. Conversely, when the steering and the target vectors differ, presence of the target will cause a shift in the weight vector. In this case, the target is interpreted as an interference and the array acts to reject it. Since in practice it is difficult to ensure that the target and steering vector are equal (no pointing error and perfect calibration), to preclude target cancellation, covariance matrix estimation is

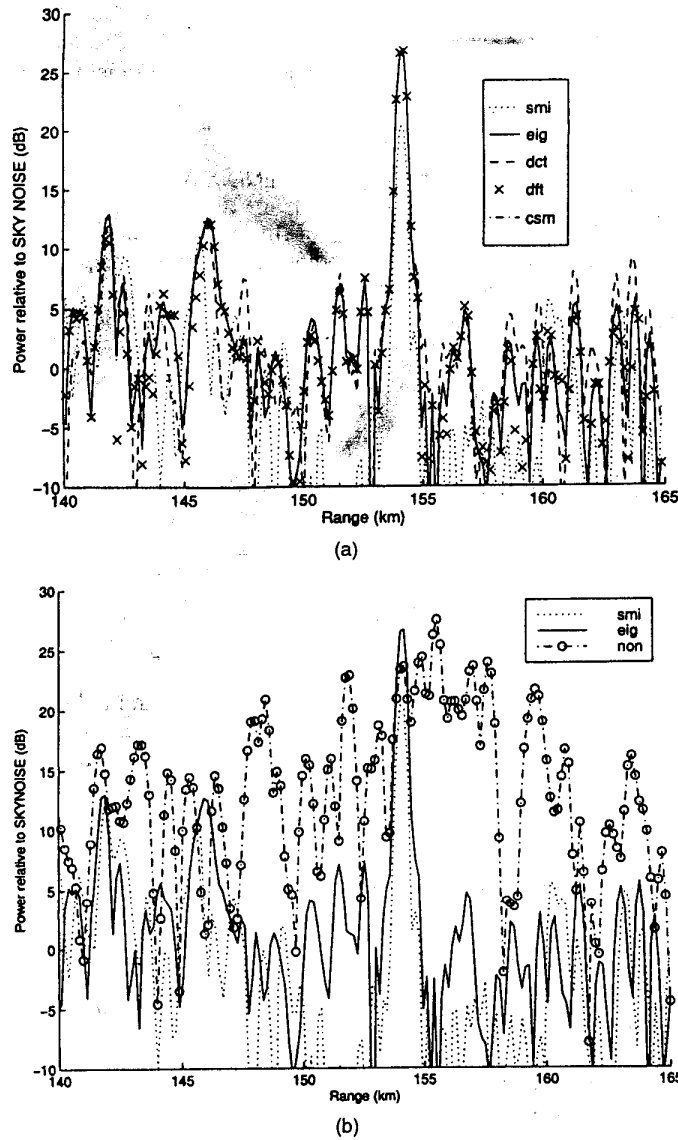


Fig. 14. Range plot of mountaintop data.

done without the range cells in the vicinity of the one tested. RR methods constrain the weight vector to the noise subspace. These methods tend to be less susceptible to the presence of the target in the training data, since a few target cells may cause no change in the interference/noise subspace partition [18]. Indeed, the covariance matrix may be expressed

$$\mathbf{R} = \frac{1}{K} \sum_{k=1}^K \mathbf{x}_k \mathbf{x}_k^H + \frac{1}{K} \sum_{m=1}^M |a_m|^2 \mathbf{ss}^H \quad (39)$$

where M is the number of range cells for which there is a target return and a_m are the target complex amplitudes. As the size of the training region (i.e., K) is increased, and since the number of range cells containing the target is kept fixed, the signal power decreases with respect to the interference. Thus at

large K , the effect of the target presence in the training data should be negligible. A measure of target cancellation at the array output is provided by the ratio r of the target power at the array output when training is done over a subset of cells including the target cell to the target power when training is done over all of the range cells. The quantity $1 - r$ measures the target cancellation relative to training over the full range interval. This quantity was computed from the Mountain-Top data, and is plotted in Fig. 16. The eigencanceler, DCT, and DFT methods exhibit lower signal cancellation than the SMI and CSM.

V. CONCLUSIONS

In this paper, the application of several RR methods was the STAP problem are examined and the

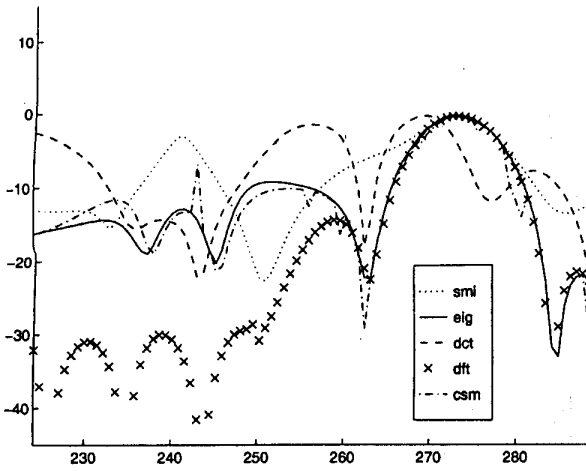


Fig. 15. Angle scan with target not included in training.

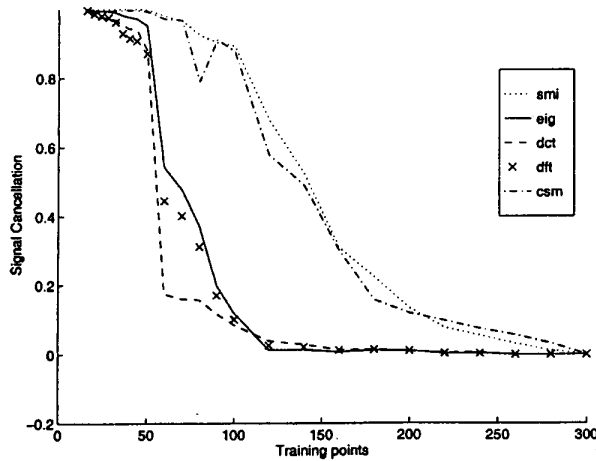


Fig. 16. Signal cancellation based on number of training points.

performance was studied by analysis of both simulations and real data. The motivation for the application of RR methods is that the STAP problem is inherently low rank. Restriction of the number of degrees of freedom through the application of RR methods has the advantage of providing robust covariance matrix estimates resulting in improved performance over SMI. A taxonomy of RR methods was presented and specific methods were analyzed.

The CSNR was defined as a figure of merit for the array performance when the interference covariance matrix is estimated from a training set. Various adaptive methods were compared according to their CSNR performance. A general expression for the CSNR density function was developed for RR methods utilizing fixed transforms. When compared with the CSNR of SMI, RR methods exhibit fewer degrees of freedom and a bias term. While the best performance of the algorithms studied here is obtained using transforms based on the eigendecomposition (data dependent), the loss incurred by the application of

fixed transforms (such as the DCT) is relatively small. The main advantage of fixed transforms is the availability of efficient computational procedures for their implementation.

APPENDIX A

In this Appendix are considered expressions (30) and (31) derived, respectively, in [15 and 16]. While there are no similarities in the derivations, it is shown here that (30) can be obtained as an approximation of (31). To that end first apply the approximation [19, p. 33 (11)]

$$\frac{\Gamma(K+1)}{\Gamma(K+1-p)} \cong K^p. \quad (40)$$

The CSNR values considered are smaller than, but close to, 1. Let $\rho = 1 - h$. Then, for $h \rightarrow 0$ and $K \rightarrow \infty$:

$$\rho^{K-p} = 1 - (K-p)h + o(h^2) \cong 1 - Kh \quad (41)$$

as well as

$$e^{-K(1-\rho)} = 1 - Kh + o(h^2). \quad (42)$$

Applying (40) and (41) in (31), and (42) in (30), we get the two expressions to be equal.

REFERENCES

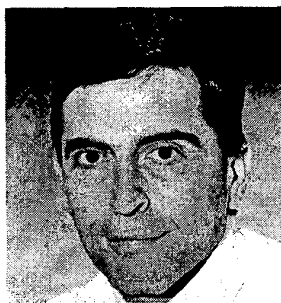
- [1] Reed, I. S., Mallett, J. D., and Brennan, L. E. (1974) Rapid convergence rate in adaptive arrays. *IEEE Transactions on Aerospace and Electronic Systems*, **AES-10**, 6 (Nov. 1974), 853-863.
- [2] Kirsteins, I. P., and Tufts, D. W. (1994) Adaptive detection using low rank approximation to a data matrix. *IEEE Transactions on Aerospace and Electronic Systems*, **30** (Jan. 1994), 55-67.
- [3] Haimovich, A. M. (1996) The eigencanceler: Adaptive radar by eigenanalysis methods. *IEEE Transactions on Aerospace and Electronic Systems*, **32** (Apr. 1996), 532-542.
- [4] Chang, L., and Yeh, C. (1992) Performance of DMI and eigenspace-based beamformers. *IEEE Transactions on Antennas and Propagation*, **40**, 11 (Nov. 1992), 1336-1347.
- [5] Abramovich, Y. I. (1981) Controlled method for adaptive optimization of filters using the criterion of maximum signal-to-noise ratio. *Journal of Communications Technology and Electronics*, **26** (1981), 87-95; translated from Russian.
- [6] Cheremisin, O. P. (1982) Efficiency of an adaptive algorithm with regularization of the sampled correlation matrix. *Journal of Communications Technology and Electronics*, **27** (1982), 69-77; translated from Russian.
- [7] Kumaresan, R., and Tufts, D. W. (1980) Data adaptive principal component signal processing. In *Proceedings of the 19th IEEE Conference on Decision and Control*, Albuquerque, NM, Dec. 1980, 949-954.
- [8] Tufts, D. W., Kumaresan, R., and Kirsteins, I. (1982) Data adaptive signal estimation by singular value decomposition of a data matrix. *Proceedings of the IEEE*, **70** (June 1982), 684-685.

- [9] Goldstein, J. S., and Reed, I. S. (1997)
Reduced-rank adaptive filtering.
IEEE Transactions on Signal Processing, 45, 2 (Feb. 1997), 492–496.
- [10] Goldstein, J. S., and Reed, I. S. (1997)
Subspace selection for partially adaptive sensor array processing.
IEEE Transactions on Aerospace and Electronic Systems, 33, 2 (Apr. 1997), 539–543.
- [11] Griffiths, L. J., and Jim, C. W. (1982)
An alternative approach to linearly constrained adaptive beamforming.
IEEE Transactions on Antennas and Propagation, AP-30, 1 (Jan. 1982), 27–34.
- [12] Marshall, D. F. (1994)
A two step adaptive interference nulling algorithm for use with airborne sensor arrays.
In *Proceedings of the Seventh Signal Processing Workshop on Statistical and Array Processing*, Quebec City, Canada, Apr. 1994, 301–304.
- [13] Abramovich, Y. I. (1990)
Analysis of direct adaptive tuning method for interference compensation systems with auxiliary linear constraints.
Journal of Communications Technology and Electronics, 35 (1990), 30–39; translated from Russian.
- [14] Goldstein, J. S., and Reed, I. S. (1997)
Theory of partially adaptive radar.
IEEE Transactions on Aerospace and Electronic Systems, 33, 4 (Oct. 1997), 1309–1325.
- [15] Haimovich, A. M. (1997)
Asymptotic distribution of the conditional signal-to-noise ratio in an eigenanalysis-based adaptive array.
IEEE Transactions on Aerospace and Electronic Systems, 33, 3 (July 1997), 988–997.
- [16] Kirsteins, I. P., and Tufts, D. W. (1991)
Rapidly adaptive nulling of interference.
In M. Bouvet and G. Bienvenu (Eds.), *High Resolution Methods in Underwater Acoustics*.
New York: Springer-Verlag, 1991, ch. 6, 220–249.
- [17] Titi, G. W. (1994)
An overview of the ARPA Mountaintop program.
In *Proceedings of 1994 Adaptive Antenna Systems Symposium*, Melville, NY, Nov. 1994, 53–59.
- [18] Haimovich, A. M., and Berin, M. (1997)
Eigenanalysis-based space-time adaptive radar: Performance analysis.
IEEE Transactions on Aerospace and Electronic Systems, 33 (Oct. 1997), 1170–1179.
- [19] Luke, Y. (1969)
The Special Functions and Their Approximations, Vol. 1.
New York: Academic Press, 1969.



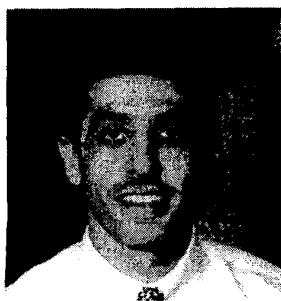
Christopher D. Peckham (S'84—M'89) received the B.S., M.S., and Ph.D. degrees in electrical engineering from the New Jersey Institute of Technology, Newark, NJ, in 1987, 1988, and 2000, respectively.

From 1990 to 1995 he was a Senior Systems and Network Administrator at the New Jersey Institute of Technology. From 1995 to 1997 he was the Director of Network Operations at Globix Corporation, New York, NY. From 1997 to early 1999 he was Manager of Network Engineering for Icon CMT, Weehawken, NJ. He is currently the Vice President of Network Engineering and Operations at Globix Corporation in New York, NY. His research interests include radar and array processing.



Alexander M. Haimovich (M'89—SM'97) received the B.Sc. degree in electrical engineering from the Technion Institute of Technology, Haifa, Israel in 1977. He received the M.Sc. degree in electrical engineering from Drexel University, Philadelphia, PA in 1983, and the Ph.D. degree in systems from the University of Pennsylvania, Philadelphia, in 1989.

From 1983 to 1987 he was a Senior Engineer with American Electronic Laboratories, Lansdale, PA. From 1987 to 1989 he was an Assistant Professor at the New Jersey Institute of Technology. He was a Senior Staff Consultant at American Electronic Laboratories from 1989 to 1990. From 1990 to 1992 he was Chief Scientist at JJM Systems, Warminster, PA. He is currently Associate Professor of Electrical and Computer Engineering at the New Jersey Institute of Technology. His research interests include adaptive array processing for radar and wireless communications.



Tareq F. Ayoub received the B.S. and M.S. degrees in electrical engineering from Manhattan College, Riverdale, NY, in 1992 and 1993, respectively. He received his Ph.D. degree in electrical engineering from the New Jersey Institute of Technology, Newark, NJ, in 1998.

He currently is a member of the technical staff at AT&T.

J. Scott Goldstein (S'86—M'88—SM'96) is a Senior Scientist at SAIC, where he serves as the Manager of the Adaptive Signal Exploitation Branch within the Sensor System Operation of SAIC's Technology Research Group. His responsibilities include program development, program management and technical leadership in advanced signal processing for detection, estimation, classification and recognition within the fields of radar, sonar, communications and navigation. In addition, Dr. Goldstein is an Adjunct Professor in the Bradley Department of Electrical and Computer Engineering at the Virginia Polytechnic Institute and State University, where his teaching and research efforts center around statistical and adaptive signal processing. He also serves as a reserve officer in the U.S. Air Force, involved in the research and development efforts for multiple sensor programs. Dr. Goldstein received his Ph.D. in electrical engineering from the University of Southern California in 1997.

From 1998 to 1999, Dr. Goldstein was a staff member at MIT Lincoln Laboratory. From 1995 to 1997, he was with the University of Southern California. From 1993 to 1997, he was the Vice-President and Chief Scientist of Adaptronics, Inc. From 1992 to 1995, he was with the Radar Systems Division of the Sensors and Electromagnetic Applications Laboratory at the Georgia Tech Research Institute. From 1990 to 1999, he was also assigned as a reserve officer with the Air Force Research Laboratory. Prior to this, Dr. Goldstein served as a signal and infantry officer in the U.S. Army and was associated with both the George Mason University Center of Excellence in C3I and the Institute for Defense Analyses. He has also served as a consultant to the Army Research Laboratory and Adaptive Sensors, Inc.

Dr. Goldstein is a member of Sigma Xi, Tau Beta Pi and Eta Kappa Nu. He is currently serving as the Assistant Administrative Editor for the IEEE Aerospace and Electronic Systems Society and is a member of the IEEE AES Radar Systems Panel. He is a recipient of the IEEE AES EASCON Award, the Japanese Okawa Foundation Research Grant and the AFCEA Postgraduate Fellowship. In addition, Dr. Goldstein has received over 15 Air Force Awards for Scientific Achievement due to his research in radar and communications.



Irving S. Reed (SM'69—F'73) was born on November 12, 1923 in Seattle, WA. He received the B.S. and Ph.D. degrees in mathematics from the California Institute of Technology, Pasadena, in 1944 and 1949, respectively.

From 1951 to 1960, he was associated with Lincoln Laboratory, Massachusetts Institute of Technology. From 1960 to 1963, he was a Senior Staff Member with the RAND Corporation. Since 1963, he has been a Professor of Electrical Engineering and Computer Science at the University of Southern California, where he currently holds the Charles Lee Powell Chair. He is also a consultant to the RAND Corporation and is a Director of Adaptive Sensors, Inc. His research interests include mathematics, VLSI computer design, coding theory, stochastic processes, information theory, image processing, and statistical signal processing.

Dr. Reed is a member of the National Academy of Engineering. He has authored and coauthored approximately 300 publications, and is the holder of six U.S. patents. He has received fourteen NASA Awards for Outstanding Technical Contributions, the USC Associates Award for Creativity in Research and Scholarship, the IEEE Aerospace and Electronic Systems Society's M. Barry Carlton Memorial Award for Best Paper, the IEEE Richard W. Hamming Medal, and the Distinguished Alumni Award from the California Institute of Technology. Dr. Reed was a Shannon Lecturer at the IEEE International Symposium on Information Theory, and was presented with the IEEE Information Theory Society's Shannon Award in 1995. He also received the 1995 Masaru Ibuka Consumer Electronics Award.

